Analysis of a Novel Mechanically Adjusted Variable Flux Permanent Magnet Homopolar Inductor Machine with Rotating Magnetic Poles for Flywheel Energy Storage System

Qing Li, *Student Member, IEEE*, Mingcheng Lyu, Jiangtao yang, *Member, IEEE and CES,* and Shoudao Huang, *Senior Member*

***Abstract*—Permanent magnet homopolar inductor machine (PMHIM) has attracted much attention in the field of flywheel energy storage system (FESS) due to its merits of simple structure, brushless excitation, and rotor flywheel integration. However, the air-gap flux generated by the PM cannot be adjusted, which would cause large electromagnetic losses in the standby operation state of FESS. To solve this problem, a novel mechanically adjusted variable flux permanent magnet homopolar inductor machine with rotating magnetic poles (RMP-PMHIM) is proposed in this paper. The permanent magnet poles are rotated by an auxiliary rotating device and the purpose of changing the air-gap flux is achieved. First, the structure and operation principle of the proposed RMP-PMHIM are explained. Second, the flux weakening principle of the RMP-PMHIM is analyzed and the equivalent magnetic circuit models under different flux weakening states are built. Third, the parameters of the PM and its fixed structure are optimized to obtain the good electromagnetic performance. Fourth, the electromagnetic performance, including the air-gap flux density, back-EMF, flux weakening ability, loss, etc. of the proposed RMP-PMHIM are investigated and compared. Compared with the non-rotating state of the PM of RPM-PMHIM, the air-gap flux density amplitude can be weakened by 99.95% when the PM rotation angle is 90 degrees, and the no-load core loss can be suppressed by 99.98%, which shows that the proposed RPM-PMHIM is a good candidate for the application of FESS.**

***Index Terms*—Homopolar inductor machine (HIM), Variable flux, Flywheel energy storage system (FESS).**

I. Introduction

ENERGY storage is an effective way for power systems to realize energy conversion, storage and utilization. Among many energy storage methods, flywheel energy storage (FES) has attracted wide attention due to its advantages of high-power density, fast response speed, long service life and environmentally friendly, etc. [1]-[3].

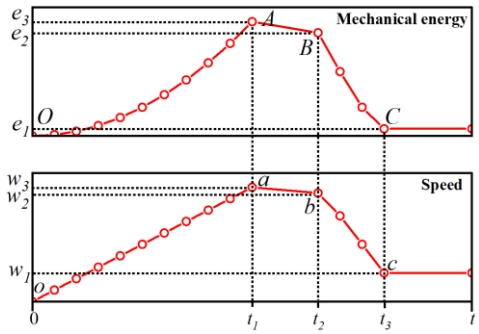

Fig. 1 Energy storage process of the PMHIM. e_i is the mechanical energy stored in the flywheel, w_i is the speed of the flywheel, and t_i is the time.

As a key component of energy conversion in the FES system (FESS), the performance of the electrical machine would directly determine the energy conversion efficiency of FESS [4]. Permanent magnet homopolar inductor machine (PMHIM) has received extensive attention in the field of FESS due to its merits such as simple structure, rotor robustness, and high efficiency [5]-[7]. However, for the difficulty of adjusting the air-gap flux generated by the PM, the PMHIM operating in the standby state would cause large no-load electromagnetic loss, which reduces the energy conversion ratio, especially in the long standby operation state. The energy storage process of the PMHIM is divided into three stages, namely charging, standby and discharging. These processes can be represented by the OA (oa), AB (ab), and BC (bc) curves in Fig. 1, respectively. When the PMHIM operates at charging state, the speed and the storage energy of rotor increases, as depicted by the curve OA (oa). When the PMHIM works at discharging state, the speed and the storage energy of rotor decreases, as depicted by the curve BC (bc). As shown by the curve AB in Fig.1, since the PMHIM would produce no-load loss in the standby operation state, the mechanical energy stored in the flywheel will gradually decrease, which leads to the reduction of the energy conversion efficiency of the FESS. The no-load loss includes the no-load electromagnetic loss, air-gap friction loss and bearing friction loss. The air-gap and bearing friction losses can

Manuscript received October 24, 2021; revised January 24, 2022; accepted March 24, 2022. date of publication September 25, 2022; date of current version September 18, 2022.

This work was supported in part by the National Natural Science Foundation of China under Grant 52007055 and in part by the Natural Science Foundation of Hunan Province of China under Grant 2021JJ40099. *(Corresponding author: Jiangtao Yang)*

Q. Li, M. Lyu, J. Yang, and S. Huang are with the College of Electrical and Information Engineering, Hunan University, Changsha, 410082, China (e-mail: qli@@hnu.edu.cn; 289763620@qq.com; yangjiangtao@hnu.edu.cn; hsd1962@hnu.edu.cn).

Digital Object Identifier 10.30941/CESTEMS.2022.00030

be eliminated by the vacuum environment and magnetic bearing, respectively [8]. The no-load electromagnetic loss is caused by the air-gap flux generated by the permanent magnet (PM). Therefore, it is necessary to adjust the air-gap magnetic field of PMHIM to suppress the no-load electromagnetic loss.

The method for changing the air-gap flux of a permanent magnet synchronous machine (PMSM) can be mainly divided into flux memory PM, hybrid excitation, and mechanical modulation method [9]-[12]. The flux memory machine uses PMs with low coercivity and high coercivity in series or parallel to provide a magnetic field. However, due to the cross-coupling effect of low-coercivity and high-coercivity PMs under load, irreversible demagnetization of low coercivity will occur at any time [13]. For hybrid excitation, the air-gap flux density is not eliminated, but some alternating components are reduced. Besides, the existence of the excitation winding would increase the excitation loss [14]. Compared with the two methods described above, mechanical modulation method has the advantages of simple structure, high reliability, and no additional loss [12].

A staggered rotor was proposed in [15] to realize the adjustable air gap magnetic field of a PMSM. Ideally, the air gap magnetic field could be completely suppressed, whereas, due to the complicated of the rotor and the control method, additional loss will be generated when the segmented rotor rotates relative to each other, which in turn affects its operating efficiency. An adaptive centrifugal device in view of the adjustable air gap magnetic field of PMSM is studied in [16]. Nonetheless, with the continuous change of the motor speed, the PMs are constantly in contact with the stator, which may affect the strength of the PMs. For the PMHIM, a mechanical ring to realize the flexible adjustment of the air gap magnetic field was proposed in [6] (hereafter, called SMM-PMHIM). However, since the mechanical ring needs to slide on the surface of the shell, the flux weakening ability of the mechanical ring will be greatly affected by the length of the oil film air gap between it and the shell. For purpose of completely suppress the air gap magnetic field, this paper proposes a new type of rotating magnetic pole PMHIM (RMP-PMHIM). By changing the PM structure of the traditional PMHIM, and adding auxiliary devices for rotating the PM to achieve the purpose of modulating the air gap magnetic field.

The rest of this paper are organized as follows. In section II, the topology and weakening mechanism of the RMP-PMHIM are explained in detail. In section III, the geometric parameters of the PM and its fixed structure parameters are optimized by the finite element method. In section IV, a comprehensive electromagnetic performance analysis of the optimized RMP-PMHIM is performed. In section V, the conclusions of this paper are drawn.

II. Topology and Operation Principle

A. Topology

The structure of the SMM-PMHIM is shown in Fig. 2(a) [6]. The PM of SMM-PMHIM is a monolithic ring, and there is a mechanical ring outside the shell for adjusting the air gap magnetic field. When SMM-PMHIM is in a completely flux weakening state, its magnetic circuit is represented by the red solid line and the dark green solid line. The existence of the mechanical ring is to provide an additional magnetic circuit for the magnetic flux generated by the PM. It should be noted that the magnetic resistance of the additional magnetic circuit is much smaller than the air gap magnetic resistance of SMM-PMHIM, which can achieve the purpose of shunting the magnetic flux generated by the PM.

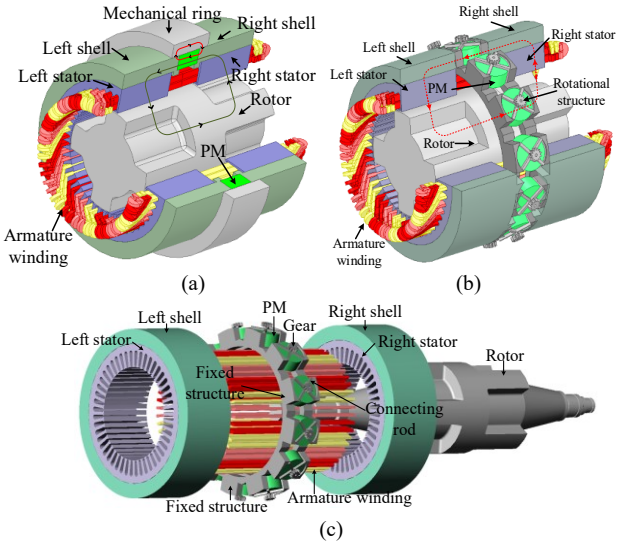

Fig. 2. Structure of mechanically adjusted variable flux PMHIM. (a). Assembly model of SMM-PMHIM. (b) Assembly model of the proposed RMP-PMHIM. (c) Explode model of RMP-PMHIM.

Figs. 2(b) and 2(c) show the assembly model and explosion model of the RMP-PMHIM, respectively. Different from the SMM-PMHIM, the PMs of RMP-PMHIM are cylindrical, and the mechanical ring is removed. The shell and the stator are coaxially installed and divided into the left and right parts. The AC windings are embedded inside the stator. The rotor has teeth and slots evenly distributed on the left and right, but the tooth axes on both sides differ by half an electrical cycle. The disc-shaped PM is rotated through a rotating structure (including gears, connecting rods, and fixed structures) to achieve flexible adjustment of its air gap magnetic field.

Fig. 3 shows the rotating structure of permanent magnet. From left to right are the assembly drawing of the rotating structure, the enlarged view of the rotating structure and local structure. The fixed shell is installed in the middle of the two-section shell and its function is to prevent the rack from moving in axial direction. There is a clearance fit between the rack and the fixed shell, so that the rack can rotate in the circumferential direction. The gear on the permanent magnet relates to the gear on the shaft of the driving motor through the rack, and the driving motor is fixedly connected with the pedestal. The drive motor rotates and drives the rack to rotate, thus driving the permanent magnet to rotate.

B. Principle of Flux Weakening

Fig. 4(a) shows the three-dimensional model of the flux weakening device, in which the PM are tightly installed with the metal shell, and the PM can be rotated along the rotating

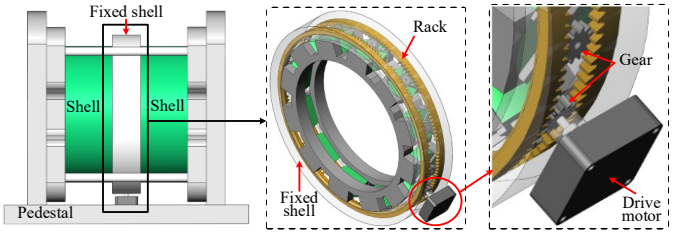

Fig. 3. Permanent magnet rotating structure of RMP-PMHIM.

shaft through gear transmission. The connecting rod is connected to the metal shell by thread. The PM rotates by the same angle as the gear rotates around the rotating axis. When the magnetizing direction of magnetic pole of the PM points to the axial direction, the rotation angle of the magnetic pole is 0 degree. Figs.4 (b), 4(c) and 4(d) show the distribution of magnetic field lines of PM at the rotation angles 0, 45 and 90 degrees, respectively. When the rotation angle is 0 degree, all the magnetic flux provided by the PM acts as the main flux to provide magnetic field for RMP-PMHIM. When the rotation angle gradually increases, take the rotation angle of 45 degrees as an example, at this time, the magnetic pole will form a contact surface with the air, which will inevitably form air-gap magnetic leakage, see Fig. 4 (c), so the flux it can provide for the RMP-PMHIM will decrease. It is worth noting that when the rotation angle is 90 degrees, the PM would no longer provide flux for the RMP-PMHIM for electromechanical energy conversion, as shown in Fig. 4 (d)

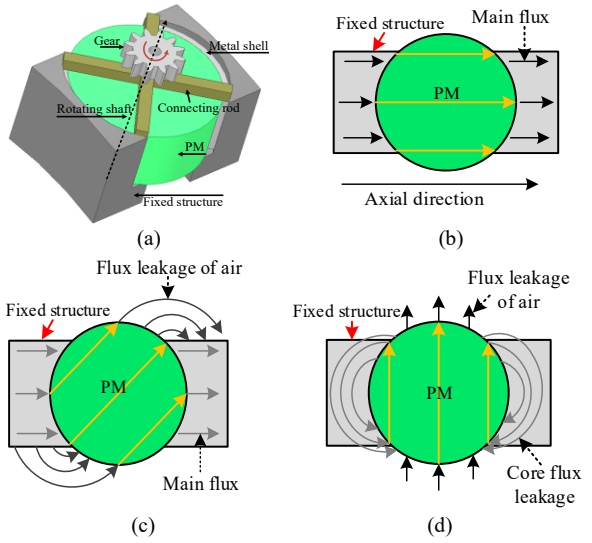

Fig. 4 Schematic diagram of permanent magnet at different rotation angles. (a) Flux weakening device. (b) 0 degree. (c) 45 degrees. (d) 90 degrees.

When the rotation angle of PM is less than 90 degrees, ignore core flux leakage, the equivalent magnetic circuit network of a single disc-shaped PM under different rotation angles can be uniformly expressed. Fig. 5 shows the magnetic circuit network of disc-shaped PM, where the PM is divided into 2*n* PMs in parallel in the magnetizing direction. Each separated PM is equivalent to a series of magnetomotive force source and magnetoresistance. As is known from observation, the magnetic circuit network shows center symmetry about the rotation axis. Therefore, only *n* branches need to be studied, and the magnetic circuit characteristics of the other *n* branches can

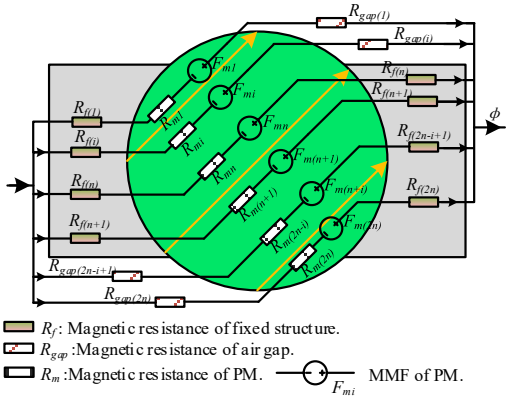

Fig. 5. Single PM circuit network of RMP-PMHIM when the rotation angle of PM is less than 90 degrees.

be obtained according to symmetry.

Assuming that there are *i* branches in series with the air magnetoresistance in *n* branches, taking the *i*-th branch as an example, the magnetic circuit network composed of this branch and the remaining components of the RMP-PMHIM can be shown in Fig.6 (a). The magnetic flux that the *i*-th pieces of PMs can provide to the RMP-PMHIM can be expressed as

$$\Phi_i = \frac{F_i}{2(R_{sh} + R_{sta} + R_{rot} + R_{air}) + R_{gap(i)} + R_{mi} + R_{f(i)}} \quad (1)$$

Therefore, the total magnetic flux generated by separated permanent magnets from the first block to the *i* block can be expressed as:

$$\Phi_{air} = \sum_{k=1}^{i} \Phi_k \quad (2)$$

where Φ_{air} represents the total magnetic flux flowing through the air, *k* represents the *k*-th separate permanent magnet, and *i* represents that there are *i* permanent magnets in series with the air reluctance.

Since the shell, stator, and other parts of RMP-PMHIM are made of materials with good magnetic permeability, the magnetic resistance of these parts can be ignored. However, for the flux linkage path shown in Fig. 4(c), the air gap length which the air leakage flux linkage passes are much larger than the main air gap length inside the RMP-PMHIM. Therefore, the magnetic flux (Φ_i) passing through the leakage magnetic circuit can be considered as 0 Wb.

The (*i*+1)-th branch is not connected in series with the air reluctance, so its simplified equivalent magnetic circuit is shown in Fig. 6(b), and the magnetic flux that the (*i*+1)-th branch can provide to the RPM-PMHIM can be expressed as

$$\Phi_{i+1} = \frac{F_{m(i+1)}}{2(R_{sh} + R_{sta} + R_{rot} + R_{f(i+1)} + R_{air}) + R_{m(i+1)}} \quad (3)$$

Therefore, the flux generated by separated permanent magnets from the remaining (*n*-*i*) blocks can be expressed as

$$\Phi_{core} = \sum_{k=1}^{n-i} \Phi_k \quad (4)$$

Assuming that the RMP-PMHIM has a total of *j* PMs, the magnetic flux generated by all *j* PMs through the RMP-PMHIM can be expressed as

$$\Phi = 2j(\Phi_{core} + \Phi_{air}) \approx 2j\Phi_{core} \quad (5)$$

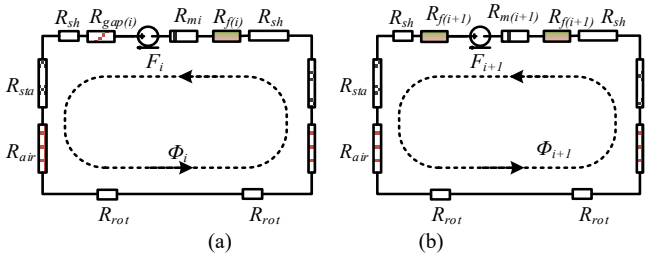

Fig. 6 Simplified magnetic circuit network formed by the separated permanent magnet. (a) i-th pieces of permanent magnets. (b) (i+1)-th pieces of permanent magnets. R_{sh} represents the magnetic resistance of shell, R_{sta} represents the magnetic resistance of stator, R_{air} represents the magnetic resistance of main air gap, and R_{rot} represents the magnetic resistance of rotor.

It can be seen from the above analysis that the greater the rotation angle of the permanent magnet, the greater the value of i, and the smaller the flux that the permanent magnet can provide for the RMP-PMHIM. In order to minimize the air gap magnetic field of RMP-PMHIM, i is preferably equal to n.

When the rotation angle of the magnetic pole of the PM is equal to 90 degrees, the separated PM in contact with the air is in open state because the air-gap reluctance is much greater than the main air-gap reluctance of the RMP-PMHIM. Equivalent network of a single PM in this state is shown in Fig. 7. The N, S poles of the separated PMs distributed on both sides are short-connected by the conductive material, so large flux leakage will be formed on both sides, but the flux leakage will not pass through the main air gap. In this state, the main air gap magnetic field of the RMP-PMHIM is completely suppressed.

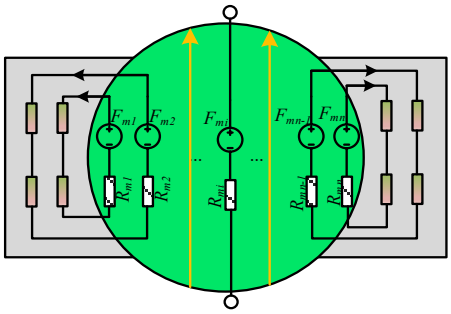

Fig. 7. Single PM circuit network of RMP-PMHIM when the rotation angle of PM is equal to 90 degrees.

The core loss of RMP-PMHIM can be calculated by [17].

$$P_v = k_h f B_m^{\ 2} + k_c (f B_m)^2 + k_e (f B_m)^{1.5} \qquad (6)$$

where k_h, k_c and k_e are hysteresis loss, eddy current loss and additional loss coefficient, respectively, f is frequency and B_m is amplitude of flux density, respectively.

Based on the above analysis, when the rotation angle of PM reaches 90 degrees, the magnetic field is completely suppressed, so the RMP-PMHIM in the no-load state would not produce electromagnetic losses.

III. Key Structure Parameters Optimization

To obtain the good electromagnetic performance of RMP-PMHIM, it is necessary to optimize its structure. Since the shell, stator, rotor, and armature winding of the RMP-PMHIM are the same as those of the SMM-PMHIM investigated in [6], only the structure parameters of the flux modulator are optimized in this paper. The thickness of PMs of RMP-PMHIM is consistent with that of SMM-PMHIM. So, there are only three parameters that can be optimized, namely the radius of the PM, the height of the fixed structure and the number of PMs.

A. Radius of PM

Increasing the radius of the PM is equivalent to increasing the excitation. Fig.8 shows the schematic diagram of the change of the radius of the PM from R_1 to R_2. Since the length of the fixed structure is L, the diameter of PM cannot be greater than L. Fig. 9 shows the back electromotive forces (back EMFs) under different PM radius when the rotation angle is 0 degree. The relationship between the back EMF and the PM radius is given in Table I. It can be found that the amplitude of the back-EMF increases as the PM radius increases. The reason is that the increase of the radius of the PM leads to the increase of the effective length of the PM in the axial direction, thus providing a large air gap magnetic field for the RMP-PMHIM. Considering the strength of the fixed structure, the radius of the PM is selected as 13 mm.

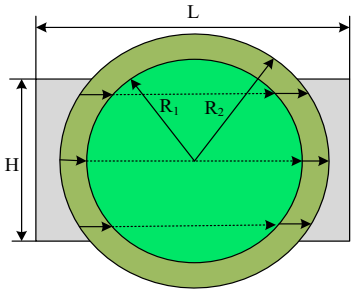

Fig. 8. Diagram of radius change of permanent magnet.

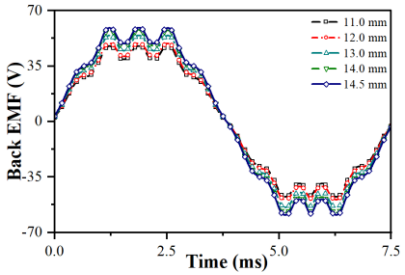

Fig. 9. Back-EMF under different permanent magnet radius when the rotation angle is 0 degree.

TABLE I
CHANGE THE RADIUS OF PERMANENT MAGNET

Parameters	Value				
Thickness of PM (mm)	10				
Radius of PM (mm)	11	12	13	14	14.5
Rotation angle (°)	0				
Number of PMs (-)	12				
Fixed structure height (mm)	20				
Back-EMF(V)	46.7	48.5	53.3	57.6	58.1

B. Fixed Structure Height

Fig. 10 shows the top view of a single PM and its fixed structure. When the height of the fixed structure is H_0, the flux flowing through the fixed structure and the PM is represented by the black dotted line with arrows (ignore the flux leakage). At this time, the region S of the PM cannot be effectively utilized. As its height increases, assuming it is H_1, the area S will be reduced, and the utilization ratio of the PM will be improved. Therefore,

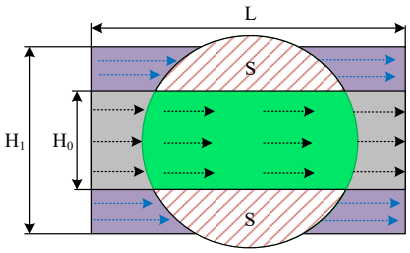

Fig. 10. Sketch of fixed structure height variation.

in order to make full use of the PM, its height needs to be optimized.

Fig. 11 shows the phase back EMF waveforms when the height of the fixed structure changes. The corresponding parameters are given in Table II. As the height gradually increases, the amplitude of the back-EMFs increases. It shows that increasing the height of the fixed structure can improve the utilization ratio of PM and the electromagnetic performance of the RMP-PMHIM, which is consistent with the previous analysis. If the height of the fixed structure is larger than the PM diameter 26 mm, the N, S pole of the PM will be short-circuited by the fixed structure, resulting in a large amount of magnetic leakage. Meanwhile, when the height is larger than 20 mm, the change ratio of the back EMF is small, so the height here is selected as 20 mm.

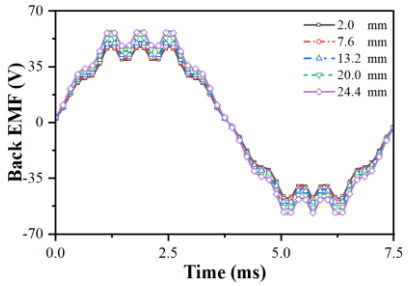

Fig. 11. Back EMF under different fixed structure height when the rotation angle is 0 degree.

TABLE II
CHANGE THE HEIGHT PARAMETERS OF FIXED STRUCTURE

Parameter	Value				
Thickness of PM (mm)	10				
Radius of PM (mm)	13				
Rotation angle (°)	0				
Number of PMs (-)	12				
Fixed structure height (mm)	2	7.6	13.2	20	24.4
Back-EMF(V)	46.7	48.1	49.9	53.4	56.6

C. *Number of PMs*

To investigate the influence of the different numbers of PMs on the electromagnetic performance the RMP-PMHIM, the RMP-PMHIM with the numbers of PMs 12 and 16 are comparatively studied. To ensure the rationality of the comparison, the back EMFs under the conditions of keeping the volume of a single PM unchanged and the total volume of the PM unchanged are compared. Due to the limitation of space, when the number of PMs increases, the radius of PMs should be reduced to avoid interference. When 16 PMs are configured, the PM radius is 12mm. When the 12 PMs are configured, the PM radius under the two states of unchanged total volume and unchanged single volume are 13.85 mm and 12 mm, respectively.

The phase back EMF waveforms of RMP-PMHIM with different PM numbers are shown in Fig. 12, and the corresponding parameters are shown in Table III. When keeping the total volume of the PMs unchanged, the back-EMF waveforms under different numbers of PMs Type I and Type III are shown in Fig. 12. Comparing the three configuration types, Type III has the best electromagnetic performance, followed by Type I, and finally Type II. However, in the Type III configuration, the fixed structure and rotating structure of the PM will become complicated, which is not conducive to the processing and manufacturing of RMP-PMHIM. The difference between Type I and Type II lies in the PM radius. Therefore, 12 PMs are selected. Comparing the back EMFs of Type I and Type II shows that the radius of the PM can be appropriately increased to improve the electromagnetic performance of RMP-PMHIM.

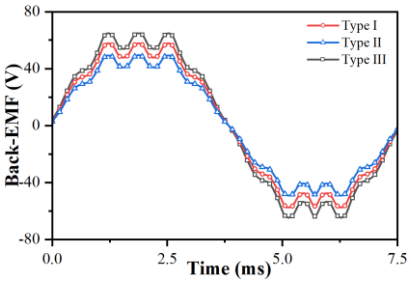

Fig. 12. Back EMF under different number of PMs when the rotation angle is 0 degree.

TABLE III
PERFORMANCE OF RMP-PMHIM WITH DIFFERENT NUMBER of PMs

Parameter	Type I	Type II	Type III
Number of PMs (-)	12	12	16
Thickness of PM (mm)	10	10	10
Radius of PM (mm)	13.85	12	12
Rotation angle (°)	0	0	0
Fixed structure height (mm)	20	20	20
Back-EMF(V)	56.3	48.5	63.1

IV. ELECTROMAGNETIC PERFORMANCE ANALYSIS

To verify the rationality of the above analysis and evaluate the electromagnetic performance of the RMP-PMHIM, the three-dimensional finite element method is adopted. The structure parameters of RMP-PMHIM and SMM-PMHIM are shown in Table IV.

TABLE IV
STRUCTURAL PARAMETERS OF SMM-PMHIM AND RMP-PMHIM

Parameter	Value	
	SMM-PMHIM	RMP-PMHIM
Outer diameter of stator(mm)	60	
Stator inner diameter (mm)	40	
Number of pole pairs (-)	4	
Main air gap (mm)	0.2	
Outer diameter of rotor(mm)	39.2	
Depth of rotor groove(mm)	12	
Number of stator slots (-)	48	
Stator core length (mm)	50	
Length of rotor (mm)	130	
Radius of PM (mm)	-	13
Number of PMs (-)	1	12

The PMs of RMP-PMHIM are independent of each other, so the way to change the air gap magnetic field of the machine can

be divided into all PMs rotating around their respective rotating shafts at the same time and each PM rotating separately.

A. Separately Rotating PMs

When there is only one PM rotating around its rotation axis, the relationship between the air-gap flux density and the rotation angle is shown in Fig. 13. As the rotation angle of the single PM is increased from 0° to 90°, the air gap flux density is reduced by 8.26%, which shows that the rotating single PM has a relatively small influence on the air gap magnetic field. Fig. 14 shows the magnitude of the torque that the PM bears during the rotation when only one PM participates in the rotation. With the gradual increase in the rotation angle of the PM, the magnetic moment it bears increases from 0 to the opposite direction, then decreases, reaches a new equilibrium position at about 75°, and then continues to increase. However, in terms of the variation range of the magnetic moment, the maximum variation of the magnetic moment is 0.46Nm in the range of 0° to 90°, which indicates that the PM can be rotated easily.

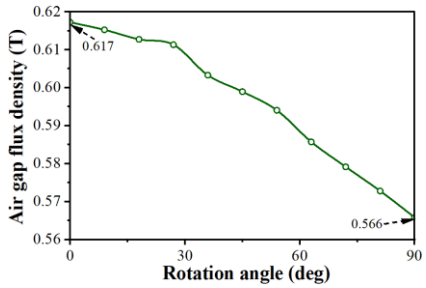

Fig. 13. Air gap flux density of a single PM under different rotation angles.

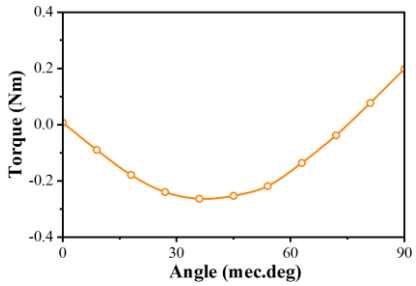

Fig. 14. The magnetic moment of a single PM when it rotates.

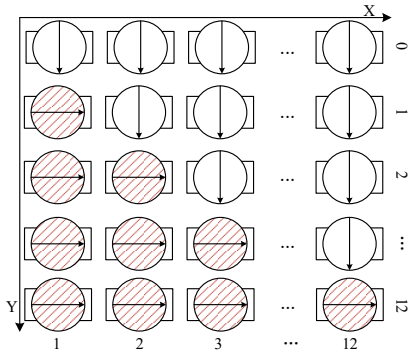

Fig. 15. Schematic diagram of PMs arranged in the circumferential direction.

To improve the magnetic field regulation ratio, the number of PMs participating in the rotation is gradually increased. It should be noted, the PMs participating in the rotation only exist in the state of 0° and 90°. Fig. 15 shows a schematic diagram of different numbers of PMs participating in rotation along the circumferential direction. The X-axis direction in the figure represents that the RMP-PMHIM is working under the current PM configuration, and the Y-axis direction represents starting from 0 and gradually increasing the number of PMs participating in the rotation until all 12 PMs participate in the rotation, the downward arrow in Fig.15 represents the axial direction, and the right arrow represents the circumferential direction.

Fig. 16 gives the relationship between the air gap flux density amplitude and the number of rotating PMs when the rotation angle of one or more PMs is 90 degrees. As the number of PMs participating in the rotation gradually increases, the air gap flux density amplitude shows a linear decrease. When all PMs are rotated to 90°, the air gap magnetic field is suppressed by 99.95%, which is consistent with the previous analysis.

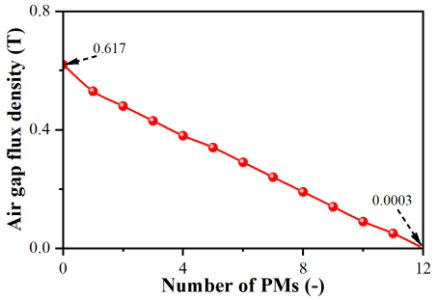

Fig. 16. The amplitude of air gap flux density varies with the number of PMs.

B. Simultaneously Rotating PMs

Fig.17 shows the distribution of magnetic field of RMP-PMHIM in the state of completely flux weakening and non-flux weakening. Comparing Fig. 17 (a) with Fig. 17(b), when the rotation angle of the PM is 90 degrees, the air gap magnetic field of the RMP-PMHIM can be greatly weakened. Fig.17 (c) and (d) are the magnetic density vector distribution of RMP-PMHIM at two different rotation angles. When the rotation angle is 0 degrees, the magnetic flux generated by the PM is all used as the main magnetic flux. However, when the rotation angle is 90 degrees, the N S poles of the PM are directly connected, which will cause a large leakage of magnetic flux, and the remaining magnetic poles are exposed to the air and do not participate in the formation of main flux.

To further observe the air gap flux density distribution of the RMP-PMHIM, Fig. 18 shows the air gap flux density of the RMP-PMHIM at different rotation angles. For the existence of the rotor teeth, the air gap magnetic density is generally rectangular. Due to the stator groove effect, the top of the waveform has a large number of tooth harmonic components. Fig. 19 shows the flux linkages of the RMP-PMHIM in different working states. It can be found that the flux linkage can be flexibly regulated.

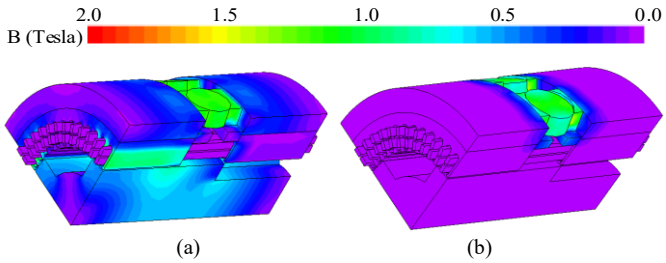

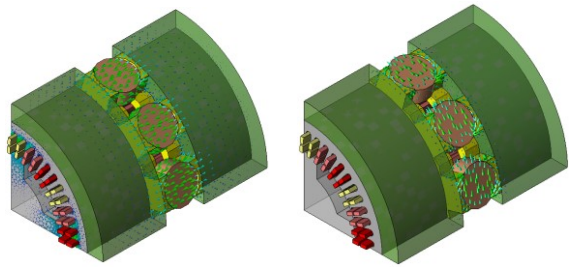

(c) (d)

Fig. 17. Distribution of magnetic field of RMP-PMHIM. (a) Magnetic field when the rotation angle is 0. (b) R Magnetic field when the rotation angle is 90. (c) Magnetic density vector distribution when the rotation angle is 0. (d) Magnetic density vector distribution when the rotation angle is 90.

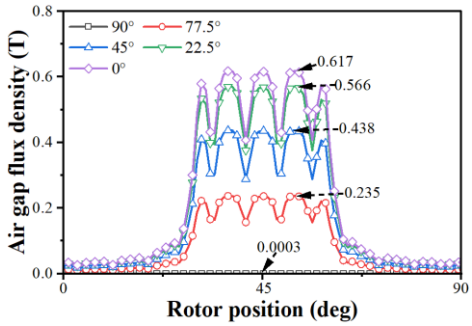

Fig. 18. The air gap flux density waveforms of the proposed RMP-PMHIM under different working states.

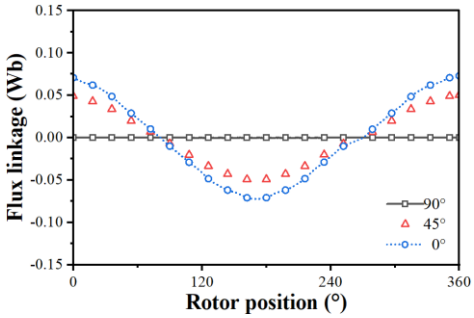

Fig. 19. The flux linkage waveforms of the proposed RMP-PMHIM under different working states.

Fig. 20 shows the no-load back EMF waveforms of RMP-PMHIM in different working conditions when the motor speed is 2000 r/min. As the rotation angle of the PMs gradually increases, the amplitude of the back EMF is gradually decreasing, and the harmonic components of the teeth at the top of the waveform are decreasing. The reason for this phenomenon may be that as the rotation angle of the PM increases, the flux weakening effect of RMP-PMHIM gradually increases, and the magnetic field saturation effect gradually decreases.

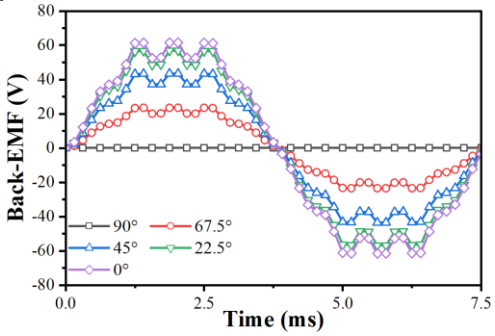

Fig. 20. The back-EMF waveforms of the proposed RMP-PMHIM.

Through the analysis of air gap flux density, flux linkage and back-EMF, it can be known that rotating PM's angle can effectively adjust the magnetic field and achieve the purpose of changing the electromagnetic performance of the RMP-PMHIM. To intuitively understand the changes in the amplitude of the back EMF of the RMP-PMHIM and SMM-PMHIM under different working conditions, the expression of the back EMF modulation ratio is defined as

$$\gamma=1-\frac{E_0}{E_{0\_\max}} \tag{7}$$

where γ is the modulation ratio of the back EMF, E_0 is the back EMF under any working state, and E_{0_max} is the amplitude of the back EMF corresponding to E_0.

Fig. 21 shows the back EMF modulation ratio of SMM-PMHIM and RMP-PMHIM in different working states, where the green curve represents RMP-PMHIM and the blue curve represents SMM-PMHIM. Comparing the two curves shows that the modulation characteristics of RMP-PMHIM are better than SMM-PMHIM.

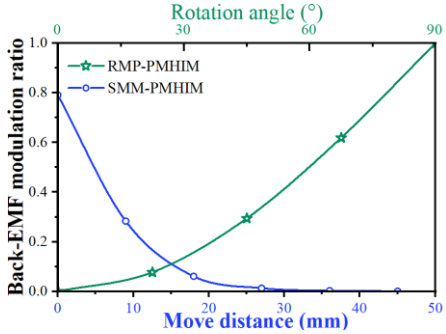

Fig. 21. Back-EMF modulation ratio of RMP-PMHIM and SMM-PMHIM

The no-load core losses of SMM-PMHIM and RMP-PMHIM are given in Fig.22, respectively. Observation shows that for RMP-PMHIM, since the PM used is less than that of SMM-PMHIM, the air gap magnetic field is weaker when the magnetic field is not weakened, so the maximum no-load standby loss is almost half of SMM-PMHIM. Meanwhile, when the rotation angle of the PM is 90 degrees, the no-load core loss is 0.001W, which shows that the no-load core loss of RMP-PMHIM can be suppressed by 99.98%.

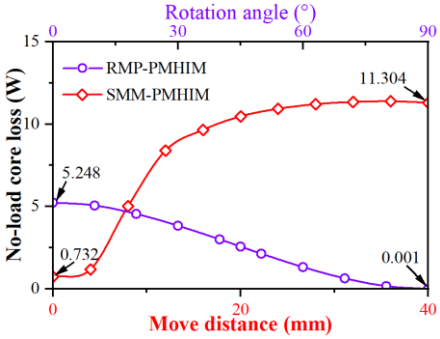

Fig. 22. No-load core loss of RMP-PMHIM and SMM-PMHIM.

Fig.23 shows the magnetic moment of a single PM when all PMs rotate. It can be seen from the figure that the change trend of the magnetic moment is first increased and then decreased with the increase of the rotation angle of PM. The point of force

balance of the PM appears at the rotation angle of 0 degrees and 90 degrees, and the point of maximum force appears near 45 degrees. Whereas, the maximum magnetic torque is not more than 1 Nm, which is beneficial to the rotation of the PM.

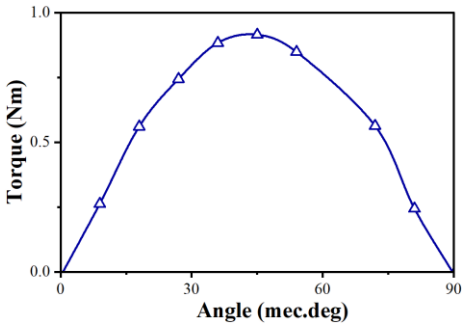

Fig. 23. Magnetic moment of a single PM when all PMs rotate.

C. Load Performance

Fig. 24 shows the schematic diagram of RMP-PMHIM in power generation state. The RMP-PMHIM is driven by the prime motor to operate at a speed of 2000 r/min. The end of the three-phase armature winding is directly connected to a symmetrical resistance load, and each resistance is 10 ohms.

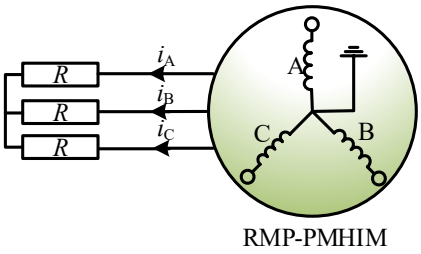

Fig. 24. RMP-PMHIM with a symmetrical resistance load.

Under the premise that all PMs participate in rotation, the phase current of the PMs at different rotation angles is shown in Fig. 25. When the rotation angle is 0°, since the air gap magnetic field of RMP-PMHIM is the largest, its corresponding armature current is the largest. With the rotation angles of 45° and 90°, the air gap magnetic field is gradually reduced, and the armature current is also reduced.

Fig. 26 shows the output power of RMP-PMHIM under different rotation degrees of PMs. As the rotation angle of the PM is 0° and 45°, the output electric power of the armature is gradually reduced due to the reduction of the air gap magnetic field. When the rotation angle of the PM is 90°, because the air gap magnetic field is almost completely suppressed, the electric power output by the RMP-PMHIM is almost 0W.

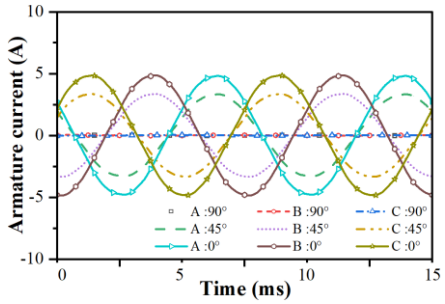

Fig. 25 Phase current.

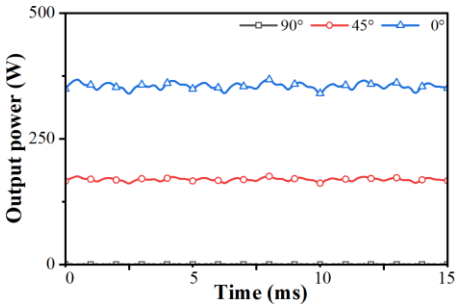

Fig. 26 Output power.

When the RMP-PMHIM is running in the power generation state, the armature current and output electric power can be ignored when the rotation angle of the PM is 90°. Table V compares the loss and efficiency parameters of the RMP-PMHIM when the rotation angle is 0° and 45°. Compared with the state where the rotation angle is 0°, when the rotation angle is 45°, the output power of RMP-PMHIM, stator core loss, rotor eddy current loss and power generation efficiency are lower.

TABLE V
DISCHARGE PARAMETERS UNDER SYMMETRICAL LOAD

Parameter	Value	
Rotation angle	0°	45°
Output power (W)	358.89	178.68
Stator core loss (W)	4.08	2.01
Rotor eddy current loss (mW)	160.4	70.3
Output current (RMS) (A)	3.39	2.33
Efficiency (%)	93.7	88.5

V. CONCLUSION

Aiming at the shortcomings of the non-adjustable air-gap magnetic field of the permanent magnet homopolar inductor machine (PMHIM), this paper proposes a mechanically adjusted variable flux permanent magnet homopolar inductor machine with rotating magnetic poles (RMP-PMHIM). The air-gap flux of the RMP-PMHIM is adjusted flexibly by rotating the magnetic poles. Firstly, the topology and flux weakening mechanism of the RMP-PMHIM are analyzed. Then, the equivalent magnetic circuits of the flux modulator under different rotation degree are built and analyzed. When the rotation degree of PM is 90 degrees, the flux generated by the PM can be almost eliminated. Moreover, to improve the electromagnetic performance of RMP-PMHIM, the structure parameters of the permanent magnet and its fixed structure, including the radium, height, number of PMs, etc. are optimized. Finally, the electromagnetic performance of the RMP-PMHIM under different rotation angles of PM is comprehensively analyzed. Compared with traditional PMHIM, the air gap flux of RMP-PMHIM could be suppressed by 99.95% and the no-load core loss can be reduced by 99.98%. The result indicates that the proposed RMP-PMHIM is a good candidate for the application of FESS. The prototype is being manufacturing and the experiment results of the prototype will be provided in future work.

REFERENCES

[1] A. A. K. Arani, H. Karami, G. B. Gharehpetian et al., "Review of Flywheel Energy Storage Systems structures and applications in power systems and microgrids," *Renewable and Sustainable Energy Reviews*, vol. 69, pp. 9-18, Mar.2017.

[2] M. Aneke, and M. Wang, "Energy storage technologies and real life applications – A state of the art review," *Applied Energy*, vol. 179, pp. 350-377, Oct.2016.

[3] T. Kousksou, P. Bruel, A. Jamil et al., "Energy storage: Applications and challenges," *Solar Energy Materials and Solar Cells*, vol. 120, pp. 59-80, Jan.2014.

[4] J. Yang, P. Liu, C. Ye *et al.*, "Multidisciplinary Design of High-Speed Solid Rotor Homopolar Inductor Machine for Flywheel Energy Storage System," *IEEE Trans. Transp. Electrif.,* vol. 7, no. 2, pp. 485-496, Jun. 2021.

[5] C. Ye, J. Yang, W. Xu *et al.*, "A Novel Multi-Unit Out-Rotor Homopolar Inductor Machine for Flywheel Energy Storage System," *IEEE Trans. Magn.,* vol. 54, no. 11, pp. 1-5, Nov.2018.

[6] J. Yang, Q. Li, S. Huang *et al.*, "Design and Analysis of a Novel Permanent Magnet Homopolar Inductor Machine with Mechanical Flux Modulator for Flywheel Energy Storage System," *IEEE Trans. Ind. Electron.,* vol. 69, no. 8, pp. 7744-7755, Aug. 2022.

[7] T. Perry, M. Senesky, and S. R. Sanders, "An integrated flywheel energy storage system with homopolar inductor motor/generator and high-frequency drive," *IEEE Trans. Ind. Appl.*, vol. 39, no. 6, pp. 1710-1725, Nov.-Dec.2003.

[8] S.Mukoyama, K. Nakao, H. Sakamoto *et al.*, "Development of Superconducting Magnetic Bearing for 300 kW Flywheel Energy Storage System," *IEEE Trans. Appl. Supercond,* vol. 27, no. 4, pp. 1-4, June.2017.

[9] Z. Q. Zhu, H. Hua, A. Pride *et al.*, "Analysis and Reduction of Unipolar Leakage Flux in Series Hybrid Permanent-Magnet Variable Flux Memory Machines," *IEEE Trans. Magn.,* vol. 53, no. 11, pp. 1-4, Nov.2017.

[10] X. Liu, M. Wang, D. Chen *et al.*, "A Variable Flux Axial Field Permanent Magnet Synchronous Machine with a Novel Mechanical Device," *IEEE Trans. Magn.,* vol. 51, no. 11, pp. 1-4, Nov.2015.

[11] Z. Q. Zhu, M. M. J. Al-Ani, X. Liu *et al.*, "A Mechanical Flux Weakening Method for Switched Flux Permanent Magnet Machines," *IEEE Trans. Energy Convers.,* vol. 30, no. 2, pp. 806-815, June.2015.

[12] J. Cekani, F. G. Capponi, G. D. Donato *et al*. (2021, Feb.), "Mechanical Flux Weakening Methods for the Achievement of a Very Wide Constant Power Speed Range in Automotive Applications," *IEEE Journal of Emerging and Selected Topics in Power Electronics,* early access: doi: 10.1109/JESTPE.2021.3058198.

[13] H. Yang, S. Lyu, H. Lin, *et al.*, "A Novel Hybrid-Magnetic-Circuit Variable Flux Memory Machine," *IEEE Trans. Ind. Electron.,* vol. 67, no. 7, pp. 5258-5268, July.2020.

[14] Z. Q. Zhu, and S. Cai, "Hybrid excited permanent magnet machines for electric and hybrid electric vehicles," *CES Trans. on Electr. Mach. Syst,* vol. 3, no. 3, pp. 233-247, Sept.2019.

[15] T. Ishii, T. Nonaka, S. Oga *et al.*, "Manufacturing and Control of a Variable Magnetic Flux Motor Prototype with a Mechanical Adjustment Method," *Electrical Engineering in Japan,* vol. 199, no. 1, pp. 57-66, Apr.2017.

[16] T. Sun, X. Liu, Y. Zou *et al.*, "Design and optimization of a mechanical variable-leakage-flux interior permanent magnet machine with auxiliary rotatable magnetic poles," *CES Trans. on Electr. Mach. Syst,* vol. 5, no. 1, pp. 21-29, Mar.2021.

[17] X. Fu, M. Lin, H. Yu *et al.*, "Calculation and Analysis of Iron Loss in Homopolar Inductor Alternator," *IEEE Trans. Magn.,* vol. 48, no. 11, pp. 3466-3469, Nov. 2012.

Qing Li (Student member, IEEE) received the B.E. degree from the Southwest University, Chongqing, China, in 2021, and now he is studying for a master's degree in the School of Electrical and Information Engineering of Hunan University, all in electrical engineering. He is currently a student with the College of Electrical and Information Engineering, Hunan University, Changsha, China.

His research interests include the design and analysis of permanent magnet motor, homopolar inductor machine, and flywheel energy storage system.

Mingcheng Lyu was born in Hunan, China, in 1990. He received the Ph.D. degree from the College of Electrical and Information Engineering, Hunan University, Changsha, China, in 2020. Since 2020, he has been a Postdoctoral Researcher with the College of Electrical and Information Engineering, Hunan University, Changsha, China.

His research interests include wind power generation technology, power quality control, and applications of power electronics.

Jiangtao Yang (Member, IEEE) received the B.E. degree from the Wuhan University of Technology, Wuhan, China, in 2014, and the Ph.D. degree from the Huazhong University of Science and Technology, Wuhan, china, in 2019, all in electrical engineering. He is currently an Assistant Professor with the College of Electrical and Information Engineering, Hunan University, Changsha, China.

His research interests include the design and analysis of high-speed electrical machine, pulsed alternator, and flywheel energy storage system.

Shoudao Huang (Senior Member, IEEE) was born in Hunan, China, in 1962. He received the B.S. and Ph.D. degrees in Electrical Engineering from the College of Electrical and Information Engineering, Hunan University, Changsha, China, in 1983, and 2005, respectively. He is currently a full time Professor with the College of Electrical and Information Engineering, Hunan University.

His research interests include motor design and control, poelectronic system and control, and wind energy conversion system.